Naval Research Laboratory

Washington, DC 20375-5000

NRL Memorandum Report 6715

Numerical Simulation of Solar Coronal Magnetic Fields

R. B. DAHLBURG, S. K. ANTIOCHOS* AND T. A. ZANG†

Center for Computational Physics Developments
Laboratory for Computational Physics and Fluid Dynamics

**E. O. Hulburt Center for Space Research*

†*NASA Langley Research Center*
Hampton, VA 23665

September 27, 1990

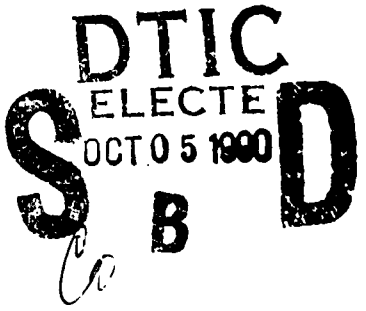

REPORT DOCUMENTATION PAGE

Form Approved
OMB No 0704-0188

1. AGENCY USE ONLY (Leave blank)	2. REPORT DATE	3. REPORT TYPE AND DATES COVERED
	1990 September 27	Interim

4. TITLE AND SUBTITLE

Numerical Simulation of Solar Coronal Magnetic Fields

5. FUNDING NUMBERS

PE - W-16 672
PR - W-16m672
TA - NASA

6. AUTHOR(S)

Russell B. Dahlburg, Spiro K. Antiochos and T. A. Zang

7. PERFORMING ORGANIZATION NAME(S) AND ADDRESS(ES)

Naval Research Laboratory
Washington, DC 20375-5000

8. PERFORMING ORGANIZATION REPORT NUMBER

NRL Memorandum Report 6715

9. SPONSORING/MONITORING AGENCY NAME(S) AND ADDRESS(ES)

National Aeronautics and Space Administration
Washington, DC 20546

10. SPONSORING/MONITORING AGENCY REPORT NUMBER

11. SUPPLEMENTARY NOTES

*E. O. Hulburt Center for Space Research, †NASA Langley Research Center, Hampton, VA

12a. DISTRIBUTION/AVAILABILITY STATEMENT

Approved for public release; distribution unlimited.

12b. DISTRIBUTION CODE

13. ABSTRACT *(Maximum 200 words)*

Many aspects of solar activity are believed to be due to the stressing of the coronal magnetic field by footpoint motions at the photosphere. We present the results of a fully spectral numerical simulation which, to our knowledge, is the first 3-d time dependent simulation of footpoint stressing in a geometry appropriate for the corona.

We consider an arcade that is initially current-free and impose a smooth footpoint motion that produces a twist in the field of approximately 2π. We then fix the footpoints and follow the evolution until the field relaxes to another current-free state. We see no evidence for any instability, either ideal or resistive and no evidence for current sheet formation. The most striking feature of the evolution is that in response to photospheric motions, the field expands rapidly upward to minimize the stress. The expansion has two important effects. First, it suppresses the development of "dips" in the field that could support dense, cool material. For the motions that we assume, the magnetic field does not develop a geometry suitable for prominence formation. Second, the expansion inhibits ideal instabilities such as kinking. Our results indicate that simple stearing of a single arcade is unlikely to lead to any solar activity such as flares or prominences. We discuss effects that might possibly lead to such activity.

14. SUBJECT TERMS		15. NUMBER OF PAGES
Solar magnetic field Photospheric motions	Numerical simulation	35
		16. PRICE CODE

17. SECURITY CLASSIFICATION OF REPORT	18. SECURITY CLASSIFICATION OF THIS PAGE	19. SECURITY CLASSIFICATION OF ABSTRACT	20. LIMITATION OF ABSTRACT
UNCLASSIFIED	UNCLASSIFIED	UNCLASSIFIED	UL

CONTENTS

NUMERICAL SIMULATION OF SOLAR CORONAL MAGNETIC FIELDS

I. INTRODUCTION

It is widely believed that the solar magnetic field is the driver for essentially all manifestations of coronal activity. Both the structure and the dynamics of coronal plasma are determined by the magnetic field. The basic idea is that photospheric footpoint motions stress the coronal field lines, thereby determining the coronal topology and producing magnetic free energy that can be converted into plasma kinetic and thermal energy. Hence, the response of the coronal magnetoplasma to footpoint motions is of fundamental importance for understanding solar activity and many other astrophysical phenomena.

In recent years there has been a great deal of work on this topic of coronal response to photospheric motions. Due to the complexity of the relevant equations, most of the effort has been on numerical simulations. We present in this paper the results of a numerical simulation that applies to the situation of twisting a flux tube in a magnetic arcade. The calculation is a dynamic, fully-three-dimensional MHD simulation in a geometry appropriate to the corona. To our knowledge this is the first one of its kind. The model and the numerical methods are described in the next Section.

Manuscript approved August 2, 1990.

The results of our simulation are pertinent to several outstanding questions in solar coronal studies. One question concerns the topology of prominence magnetic fields. It is commonly believed that the cool, dense, H_α emitting material in high quiescent prominences must be supported by the magnetic field (e.g. Tandberg-Hanssen 1974). In that case the magnetic field lines must form a "hammock" shape in the corona so that the cool material can rest at the bottom of the hammock. Several hammock-type models have been proposed (e.g. Kippenhahn and Schlüter 1957, Kuperus and Raadu 1974). The key question is, how does the field obtain such a geometry? A single current-free arcade has field lines that are concave-down in the corona. Perhaps the simplest and most appealing explanation is that photospheric motions twist the field lines of an initially current-free flux tube into the appropriate shape. Parker (1979) has shown that the twist will tend to propagate to the weakest part of the field, near the apexes of the flux tube. If sufficient twist is introduced, (of order one complete rotation or more), and if the twist is sufficiently localised at the apex, then some of the field lines must acquire a concave-up geometry. Analytic models for such a twisted flux tube have been constructed by several authors (e.g. Démoulin and Priest 1989). However, the analytic models consider only an equilibrium flux tube in isolation and only for linear departures from a 2-dimensional equilibrium. They do not consider the effect of a realistic arcade structure for the field, the dynamic formation of the twists and the effect of instabilities. Our simulation allows us to study all these topological effects.

The role of ideal instabilities is an important issue in models for coronal activity. Since many observed phenomena such as prominence eruption, sprays and coronal mass ejections exhibit mass motions with velocities of the order of the coronal Alfvén speed, it seems likely that they involve an ideal instability such as a kink. The basic idea is that if the coronal field is stressed sufficiently by photospheric motions, it becomes unstable and erupts outward carrying coronal and chromospheric plasma with it (e.g. Sturrock 1989). Two recent 3-d simulations seem to support this scenario (Strauss and Otani 1988; Mikić 1990). These authors found that continuous twisting of a flux tube eventually resulted in a kink instability. However, their simulations were performed for a geometry in which the field is confined between two vertical plates and the system has cylindrical symmetry (before kinking). These constraints permit the buildup of arbitrarily large stresses. In the true coronal geometry the field is free to expand upward and there is no symmetry to the field. Hence the coronal magnetic field can relax gradually in response to photospheric motions. It is not clear if kinking will occur in this case as well, hence, more simulations are needed to determine whether ideal instabilities occur in more realistic coronal magnetic fields.

Another issue is the role of magnetic reconnection. A number of authors (e.g. Pneuman 1983, Moore 1988, Sturrock 1989, Van Ballegooijen and Martens 1989, etc) have invoked reconnection in a sheared arcade as a mechanism for both the formation and eruption of prominences. The concept underlying their models is that reconnection can redistribute the shear in an arcade such that part of the arcade flux becomes less sheared

while another part becomes progressively more sheared. In their model reconnection has the effect of concentrating the shear in a certain flux region. It is this highly sheared flux that eventually erupts, and leads to flares (Moore 1988). This is a very promising model. Simulations on a reduced two-dimensional model, coupled with the assumption that the reconnection did rearrange the shear as postulated, do show prominence eruption (Van Ballegooijen and Martens 1989). The full three-dimensional model has yet to be verified by rigorous calculations. However, there are serious doubts as to whether true reconnection (as opposed to simple diffusion) can ever take place in a coronal arcade. Linear theory (e.g., Velli and Hood 1986) indicates that resistive tearing is suppressed by line-tying in a field that does not have a reversal of the unsheared initial field, as is the case for a dipole arcade. In the general non-linear regime, Greene (1988) has presented arguments for the absence of reconnection in a field with the topology of a single arcade. Hence, we believe that the role of reconnection in a coronal arcade is an open question which detailed, 3-d simulations can help to resolve.

A related issue concerns the formation of DC electric current sheets in closed magnetic configurations in the solar corona. Current sheets are very important for models of coronal heating. In order to account for the observed energy losses, it is widely believed that the electric currents in the corona must attain a highly filamented structure as in a current sheet. Parker (1972, 1987) proposes that current sheets form as a natural consequence of footpoint motions. He argues that a general 3-dimensional magnetic field such as that in the corona can have no well-behaved equilibrium state, and that magnetic singularities

corresponding to current sheets must form to allow the magnetic field to relax to a lower energy state. Several authors have numerically tested this hypothesis using 3-dimensional force-free-field codes (Van Ballegooijen 1988, Mikič et al, 1989). They concluded that their calculations did not support Parker's hypothesis. These calculations, however, were performed for an initially uniform field confined between two plates. Our arcade geometry is more appropriate for the corona, and we include the dynamics, so that we can examine different aspects of the current-sheet formation question than the equilibria codes.

In the next section we describe the exact model that we use for the simulation and our numerical code. The final section discusses the results and our conclusions.

II. THE SIMULATION MODEL

a) The Numerical Code

We begin with the dissipative, incompressible magnetohydrodynamic (MHD) equations, written in a dimensionless rotation form:

$$\frac{\partial \mathbf{v}}{\partial t} = \mathbf{v} \times \boldsymbol{\omega} - \nabla \Pi + \mathbf{j} \times \mathbf{B} + \frac{1}{M} \nabla^2 \mathbf{v}, \tag{1a}$$

$$\nabla \cdot \mathbf{v} = 0, \tag{1b}$$

$$\frac{\partial \mathbf{A}}{\partial t} = \mathbf{v} \times \mathbf{B} + \nabla \Phi - \frac{1}{S} \nabla \times \nabla \times \mathbf{A}. \tag{1c}$$

and,

$$\nabla \cdot \mathbf{B} = 0, \tag{1d}$$

where $\mathbf{v}(\mathbf{x},t) = (u,v,w) \equiv$ flow velocity, $\boldsymbol{\omega}(\mathbf{x},t) = \nabla \times \mathbf{v} \equiv$ vorticity, $\mathbf{A}(\mathbf{x},t) \equiv$ magnetic vector potential, $\mathbf{B}(\mathbf{x},t) = \nabla \times \mathbf{A} \equiv$ magnetic field, $\mathbf{j}(\mathbf{x},t) = \nabla \times \mathbf{B} \equiv$ electric current density, $\Pi(\mathbf{x},t) \equiv$ mechanical pressure + kinetic energy density, $\Phi(\mathbf{x},t) \equiv$ magnetic scalar potential, $S \equiv$ Lundquist number, and $M \equiv$ viscous Lundquist number. Lundquist numbers are Reynolds-like numbers, with the Alfvén speed used for the characteristic velocity. We choose a gauge with $\Phi = 0$. In this representation, $\mathbf{B}$ is measured in terms of a characteristic field strength, *e.g.*, $B_0 = \left(V^{-1}\langle \mid \mathbf{B} \mid^2 \rangle\right)^{\frac{1}{2}}$, where the brackets $<>$ indicate an integral over the system and V denotes the volume of integration. The velocities are measured in units of the Alfvén speed, $C_A = B_0/(4\pi\rho)^{\frac{1}{2}}$ where the mass density, ρ, is assumed to be constant and uniform. For a characteristic distance, L_0, the time is measured in units of the Alfvén transit time, L_0/C_A. The Lundquist number $S = C_A L_0/\eta$, where η is the magnetic diffusivity. The viscous Lundquist number $M = C_A L_0/\nu$, where ν is the kinematic viscosity.

For the simulation reported here, $\eta = .0025$ and $\nu = .2$ so that $S = 500$ and $M = 5$. The low viscous Lundquist number was chosen to damp out fluid motions. In addition, it helps to dissipate small-scale magnetic structure *via* the Alfvén effect, allowing us to perform fully 3D numerical simulations at a relatively large magnetic Lundquist number. However, such small values for the Lundquist numbers might be thought to preclude magnetic reconnection *a priori*. To establish the possibility of reconnection at these Lundquist numbers, we have examined several linear and nonlinear problems where we have previously observed magnetic reconnection. One such case is the linear magnetic reconnection

problem, which reduces to the MHD version of the Orr-Sommerfeld equation (Dahlburg *et al.*, 1983, 1986). For the mean magnetic field $B_x(z) = \tanh(z)$, we find that linearly unstable modes do exist at these Lundquist numbers. In terms of the wavenumber parallel to the mean magnetic field, α, and the growth rate, ω_i, we find, for example; $(\alpha, \omega_i) =$ (0.5, 0.01), (1.0, 0.028057), (2.0, 0.03878), (3.0, 0.02255), and (4.0, 0.0096). This implies that linear instabilities are at least possible at these Lundquist numbers. We have also considered a highly nonlinear initial value reconnection problem, the Orszag-Tang vortex, at these Lundquist numbers (Orszag and Tang 1979, Dahlburg and Picone 1989). Reconnection occurs within less than one Alfvén transit time, with the attendent formation of electric current sheets and vortex quadrupoles, in a manner similar to previously reported numerical simulations of this configuration. Hence we also conclude that nonlinear magnetic reconnection can occur at these Lundquist numbers. We have also run parts of the magnetic arcade simulation reported in the present paper with a smaller viscosity, $M = 30$, and have found no significant qualitative change in the results. Let us emphasize that these Lundquist numbers, although large by the standards of numerical simulations, are still many orders of magnitude smaller than the expected solar values; hence, the simulations are bound to be much more diffusive than the real corona.

Equations 1 are solved in a three-dimensional Cartesian geometry. We employ the following numerical algorithm to discretize the equations: A Fourier pseudospectral discretization is used in x and y, the periodic directions. Chebyshev collocation is implemented in the z direction, with the mechanical pressure evaluated on a grid staggered in z.

The temporal discretization is a low-storage, third-order, Runge-Kutta – Crank-Nicolson scheme, with a backward-Euler pressure correction at each time-level (Zang and Hussaini 1986). For a grid of 32^2 Fourier modes and 32 Chebyshev modes the code requires about 2 seconds per time step on the NRL CRAY X-MP, and approximately .8 million words of memory. More details on the algorithm are given in the appendix.

b) The Initial and Boundary Conditions

Since the code requires periodicity in the x and y directions we pick as the initial field a periodic array of current-free arcades. The initial vector potential is given by:

$$A_x = A_z = 0, \tag{2a}$$

$$A_y = \cos kx \exp\left(-k(z+1)\right), \tag{2b}$$

and the computational domain consists of $0 \leq x \leq 2\pi, 0 \leq y \leq 2\pi, -1 \leq z \leq 1$. This is the same potential field studied in 2.5 dimensions by Mikić *et al.,* 1988 who considered the evolution of this field under the influence of photospheric shear flows. The initial field has translational symmetry along the y direction; however, this symmetry is broken immediately by the flow imposed at the bottom boundary of the computational box, which is supposed to correspond to the photosphere. Unlike previous calculations (Mikić *et al.,* 1989, Van Ballegooijen 1988) which focused on equilibrium states, we concentrate on coronal dynamics and do not attempt to obtain an equilibrium or steady-state. Our simulation consists of two distinct periods, a "driving" part during which free energy is built up in the coronal magnetic field by footpoint motions, and a "decay" part during which the field

relaxes back to a current-free state. The field is first twisted with a prescribed footpoint motion for 10 characteristic time scales τ, where τ is the average Alfvén crossing time for the whole system. Then the footpoint positions are fixed, and the system is allowed to evolve for another 60τ. During the driving period, $t < 10\tau$, the horizontal velocities at the bottom wall $z = -1$ are assumed to be,

$$v_x = \frac{\partial \psi}{\partial y} \qquad \text{and} \qquad v_y = -\frac{\partial \psi}{\partial x}, \tag{3}$$

where ψ is given by,

$$\psi = C \sin^2 2kx \sin^3 ky, \tag{4}$$

and C is a constant. Of course during the decay period, $t \geq 10\tau$, $v_x = v_y = 0$. Note that the form (3) for the footpoint flow corresponds to an incompressible twisting motion. The bottom wall is also assumed to be impenetrable, so that $v_z = 0$ throughout the simulation. The boundary conditions at the other walls are straightforward. At the sides of the computational box we must assume periodic boundary conditions. The top wall, $z = 1$, is assumed to be a rigid, impenetrable surface, consequently $\mathbf{v} \equiv 0$ there.

The only other quantity that requires boundary conditions is the vector potential $\mathbf{A}$. Again periodic conditions are imposed at the sides. The top and bottom conditions on $\mathbf{A}$ are selected so that the evolution at the boundary corresponds to ideal flow. However, this determines only the horizontal components of $\mathbf{A}$,

$$\frac{\partial A_x}{\partial t} = v_y B_z, \tag{5a}$$

$$\frac{\partial A_y}{\partial t} = -v_x B_z, \tag{5b}$$

where we have used the fact that v_z vanishes on the boundary. In principle, no boundary conditions need be imposed on A_z, but since the numerical code requires them, we simply solve the partial differential equation for A_z at the boundary (*cf.* Mikić *et al.*, 1988).

$$\frac{\partial A_z}{\partial t} = (\mathbf{v} \times \mathbf{B})_z - \frac{1}{S} j_z. \tag{5c}$$

We have also tried extrapolating its value from the interior, but the results are not sensitive to this assumption.

Due to the combination of the periodicity restriction and the particular problem under consideration, there is an unavoidable redundancy in the calculations. There are two arcades in the computational box, one full arcade with its neutral line at the center of the box, $x = 2\pi/6$, and one half arcade on either side. Throughout the simulation we found that both arcades behave identically, (as they should); hence, we will only show the central arcade in the following figures. This redundancy will not be present in calculations with more realistic magnetic fields and photospheric flows. For example, the photospheric flow pattern is perhaps best represented as a random, time evolving flow-field. Such a photospheric flow pattern would break the symmetry implied by equations 2 and 4.

The value of C in equation (4) for the twisting motion is chosen so that the maximum velocity at the photosphere is approximately 1/10 of the coronal Alfvén speed. Of course, this ratio for the driving speed to the characteristic velocity is much greater than in the

solar case. Typical photospheric velocities are of order 1 km/s and coronal Alfvén velocities $\sim 1,000\ km/s$ so that the actual ratio should be of order 10^{-3}. However, it is not possible to use such a low ratio in the numerical simulations because diffusion is so much stronger in the simulation model than on the real Sun. If the driving speed is too low, then the effects of the footpoint motions will diffuse away before any twist can be built up in the coronal magnetic field; the field is able to "slip" back faster than it is driven. Also, since the time step in the code is set by the characteristic velocity, it is simply too expensive computationally to use a very low ratio. A value of $\sim 1/10$ is about the smallest that can be used with our present code. This implies that our results during the driving period are likely to be too dynamic compared to the solar corona; however, the simulation should be accurate for the decay phase.

In Figure 1a the stream lines of the photospheric driving flow, equivalent to constant contours of ψ, are shown, and in Figure 1b, contours of the velocity magnitude, $|\mathbf{v}| = \left[(\partial\psi/\partial x)^2 + (\partial\psi/\partial y)^2\right]^{\frac{1}{2}}$. The flow pattern has been chosen so that the velocity vanishes at the boundary between adjacent arcades and at the neutral line of each arcade. This ensures that each arcade retains its identity; there is no mixing of flux between different arcades or between opposite polarity regions. From Figure 1 we note that the velocities are quite concentrated and are oppositely directed on either side of the neutral line so that they correspond to twisting a fairly localized flux region. Again due to the periodicity requirement there is a redundancy in the velocity pattern, consequently we have

two regions of twisted flux. They behaved identically throughout the simulation, which lends confidence in the numerical code.

The footpoint displacements that result from the photospheric velocities are shown in Figure 2, where we plot the contours of constant B_z on the bottom wall at the beginning and the end of the driving period, $t = 10\tau$. Note that from equation (2) the initial photospheric flux $B_z = -k \sin kx$ so that the initial contours are straight lines parallel to the y axis (Figure 2a). From the ideal induction equation one finds that B_z is convected with the flow for an incompressible horizontal motion,

$$\frac{\partial B_z}{\partial t} + \mathbf{v}_{ph} \cdot \nabla B_z = 0, \tag{6}$$

where $\mathbf{v}_{ph}$ is the horizontal velocity at the photosphere. Hence, by following contours of B_z one can track the footpoint positions.

There are several important features of Figure 2. It clearly demonstrates the point that for ideal motions the topology of the coronal field can be determined from the boundary conditions at the photosphere. The fact that the coronal field has been twisted is obvious from the photospheric contours. Even if the footpoint motions were much more complicated, involving winding or braiding patterns and compressible flow, the topology would be recoverable from the contours of the Euler potentials for $\mathbf{B}$ at the photosphere (Antiochos 1987,1990). It is also evident from Figure 2 that due to the footpoint motions, the B_z contours have been "stretched out", and become more concentrated. We conclude that the gradients in the footpoint displacements increase with time and, therefore, the

scales of the magnetic structures in the corona must decrease with continued twisting (e.g. Van Ballegooijen 1988, Mikić *et al.*, 1989). Note that this occurs even if the scales of the photospheric velocities remain constant. This result implies that a photospheric velocity with large scales such as that given by (4), will eventually produce structure on the photosphere, (and consequently in the corona), with scales below the numerical resolution. The actual magnitude of the twisting is evident in Figure 2. Each side of the arcade has been twisted through a maximum angle $\sim 180°$, so that the total twist is approximately one full rotation, which is about the maximum twist that we can resolve with a 32^3 grid. In order to resolve a more complicated motion such as a braiding pattern which requires at least three rotations (Antiochos 1990), we would need a much larger grid.

III. RESULTS OF THE SIMULATION

The evolution of the magnetic field lines during the simulation are shown in Figures 3a – 3d (side view), and 4a – 4d (top view). We plot two sets of field lines at four times during the run, $t = 0,\ 10\tau,\ 20\tau,$ and 70τ. These field lines were chosen by the position of one of their footpoints on the photosphere. We selected two rows of 17 points lying on the photosphere, and then traced the field line emanating from these points. The two rows are parallel to the y axis and pass approximately through the center of the twisted region of the arcade. In the Figures, these points are to the left of the photospheric neutral line which lies at the center of the grid, ($x_i = x_{17}$). Field lines with footpoints on the inner row are shown as dotted lines, those on the outer are solid.

Figures 3a and 4a show the initial current-free magnetic field (equation 2). The translational symmetry along the y direction is apparent. The field clearly has a very simple topology with all of the field lines from the inner row of footpoints lying well under the lines from the outer row. Figures 3b and 4b shows the field at the end of the driving phase, $t = 10\tau$, when it has the maximum twist. It should be noted that these are not the same field lines as in 3a and 4a. The field lines of Figures 3a and 4a have moved from their original positions so that their leftside footpoints no longer lie on our two straight rows (see figure 2). However, there is nothing special about the particular field lines in 3a and 4a, and we find it easier to see the effect of the motions by keeping a fixed, two-straight-rows pattern for the leftside footpoints in all the figures.

Comparing 3a,4a and 3b,4b it is evident that the field topology becomes much more complex as a result of the twisting. The field lines now wrap around each other so that there is no clear distinction between an outer and an inner set on the right hand side of the photospheric neutral line. The most striking feature of the twisted field lines is that they are all greatly expanded upward from the current-free positions. This result is expected from studies of force-free fields (e.g., Aly 1984; Yang, Sturrock and Antiochos 1986). The field acts to minimize any stress due to footpoint motions by expanding outward in the corona. Note that this effect is not incorporated in models with an initially uniform field confined between two horizontal plates (e.g., Parker 1972, Mikič *et al.*, 1989). For a given footpoint motion, such models will yield fields with finer current structures than in a more realistic open coronal geometry. In fact, our results also underestimate the outward expansion.

The boundary conditions that we assume at the top and bottom of an impenetrable wall, and the restriction to incompressible flows, equation (1b), all act to suppress an outward expansion.

The expansion plays a crucial role in determining the field's structure and dynamics. We note from Figures 3b and 4b that all the field lines are concave down in the corona. There are no "dips" suitable for supporting cool prominence material. If the field lines had not expanded upward, we believe that dips would have formed. The reason for the lack of dips is that outward expansion tends to decrease the pitch of field lines as they twist around each other. It seems likely that more twisting will eventually produce dips, on the other hand, Aly (1984) has argued that continual stressing of the field should lead to an open arcade. If so then even infinite twisting will not produce dips in the corona. Unfortunately, our simulation is not capable of accurately treating more than about one rotation so that we cannot address this interesting question at present.

The topology of the field lines at later times is shown in Figures 3c – 3d and 4c – 4d. Since the footpoints are held fixed during this phase of the evolution, then these field lines would correspond exactly to those in 3b,4b if the evolution were ideal. It is evident from the Figures that the evolution is far from ideal. The right-side footpoints are clearly changing with time even though we allow no flow on the boundary. The reason for this is resistive diffusion, which permits the field lines to "slip" back to their current-free positions. It is important to emphasize that this slippage is not a boundary effect; it is occurring throughout the corona. On the contrary, at the boundary the code is able to

ensure an ideal, perfectly rigid plate; but in the interior volume the code must use a finite resistivity. Note that this slipping is not unphysical; it also occurs in the real corona, but at a much slower rate.

We find that the evolution throughout the decay phase is one of simple diffusion. It is evident from Figures 3 and 4 that all the field lines tend to untwist. There is no evidence for any type of instability, ideal or resistive. This can be seen from plots of the global quantities. We show in Figure 5 the evolution during the whole simulation of the logarithm of the kinetic energy ($E_v = 1/2\langle|\mathbf{v}|^2\rangle$), the magnetic energy ($E_B = 1/2\langle|\mathbf{B}|^2\rangle$), and the mean square electric current ($J = 1/2\langle|\mathbf{j}|^2\rangle$). The forcing at the wall causes E_v to build rapidly to a saturation level. The kinetic energy decreases rapidly, due to the high viscosity, at the end of the driving phase ($t = 10$)and remains small thereafter. Growth of E_v, typically seen when jets form as a result of reconnection (*e.g.* Dahlburg, Dahlburg,and Mariska 1988), is not observed. The magnetic energy, E_B, also grows quickly during the forcing phase to about 1.5 times its initial value. After the forcing is cut off at $t = 10$, E_B exhibits a smooth monotonic decay to a level below its initial value. This reflects the fact that the magnetic field relaxes to a different equilibrium, consistent with the new footpoint positions exhibited in Figure 2b. In the same way, J increases during the forcing phase, as the forcing creates smaller spatial scale structures in the magnetic field. During the damping phase, J decays to near zero, indicating the relaxation of the magnetic field to a nearly potential state.

The nature of the magnetic field evolution can be described in terms of an effective magnetic Lundquist number, given by

$$S(t) = -\frac{2\langle|\mathbf{j}|^2\rangle}{\frac{d}{dt}\langle|\mathbf{B}|^2\rangle}. \tag{7}$$

This is also shown in Figure 5. We obtain $S(t)$ by considering the magnetic induction equation in the limit of negligible velocity, taking the scalar product of this equation with $\mathbf{B}$, and integrating the resulting magnetic energy density equation over the system. Solving for the Lundquist number gives the desired result. Figure 5d shows that $S(t)$ returns rapidly to the predicted Ohmic rate, *viz.*, $S(t) = 500$, when the forcing stops at $T = 10\tau$. The "jiggling" in the data is due to small errors in computing the denominator of $S(t)$, which is postprocessed. Since the magnetic energy fails to decay at a higher rate, magnetic reconnection must be absent.

Another important result of our simulation is that it shows no evidence for current sheet formation. Hence, our results are consistant with the studies of force-free equilibria (Sakurai 1979; Van Ballegooijen 1988; Mikić *et al.*, 1989). The lack of current sheet formation can be seen from the evolution of J shown in Figure 5. Not only does the integrated current exhibit a monotonic decay, but we have also examined in detail the spectrum of the current density, and have found that the spectrum decays as would be expected for pure resistive diffusion.

IV. DISCUSSION

The results presented in this paper are of a negative character, *i.e.*,, we do not see magnetic reconnection, kinking, or the formation of concave-up magnetic field lines suitable for prominence formation. Hence, it appears that, contrary to many models, photospheric twisting of a single arcade does not lead to the type of processes required to explain solar activity. The key question is whether this conclusion is valid in general, or whether it is due solely to the limitations of this particular simulation. The numerical simulation itself has three major shortcomings. First, it is too diffusive, especially when compared to the real corona. There is little that can be done about this problem. Larger Lundquist numbers can be obtained by going to larger grids, but there is no hope at present for obtaining numbers significantly larger than ~ 1000. Second, the numerical resolution is barely adequate. At the time of maximum twist, 10τ, the current spectrum shows a decrease of only 4 orders of magnitude over the wavenumber range. Ideally, we would like to have at least a 6 orders of magnitude decrease. Since we have used only a 32^3 grid, and much larger grids are possible on present computers, we see no difficulty in obtaining substantially better resolution in future simulations. A third problem is the incompressibility assumption. This is not valid for the solar corona; but, we believe it has not had a significant effect on the results. If anything, a compressible simulation should exhibit an even larger upward expansion and less of a tendency to instability.

There are also limitations with the assumed form for the photospheric motions. We believe that the magnitude of the twisting is sufficient. It is evident from Figure 5b that the magnetic free energy is 50% the energy of the potential field. Also it can be seen from Figures 3b and 4b that the field lines are strongly twisted. Coronal loops rarely appear to be so distorted. Although the magnitude of the motions is acceptable, their size scale is limited. Due to the difficulty with obtaining adequate numerical resolution, we have considered only a large-scale twisting in which the width of the twisting motion is approximately equal to the width of the arcade. This situation would correspond to a large-scale shearing of a coronal arcade, and is the easiest to resolve numerically. However, the photosphere also contains small-scale motions such as granular motions, for example. It may be that the small-scale motions play a crucial role in processes such as the formation of prominence dips. Simulations with larger grids are needed in order to address this possibility.

Even though our simulation is clearly limited, we believe that at least some of the results will hold for general footpoint motions and Lundquist numbers. In particular, we expect that for a dipolar magnetic arcade, resistive instabilities will not occur due to the effect of line-tying, irrespective of the footpoint motions. This argues against the reconnection scenarios proposed by a number of authors. We also expect that, contrary to the non-equilibrium model, current sheets will not form. Of course the scale of the currents in the corona is determined by the scale of the footpoint displacements, so that if the displacements have a very fine scale, then fine scale currents will result. However,

our simulation and all the equilibria calculations (Sakurai 1979; Van Ballegooijen 1988; Mikić *et al.*, 1989) find that for well-resolved footpoint displacements smooth current distributions result.

The question of ideal instabilities and the formation of concave-up field lines is less clear. We find that both are suppressed by the outward expansion of the field. Such an expansion will occur for any form of footpoint motions, but it is possible that strong, highly-localised twisting can lead to the formation of concave-up field lines and to kink-like instabilities in small regions of the arcade. If so, then small scale motions may have important consequences for prominence formation and coronal dynamics. This issue requires further study.

The general conclusion of our results is that photospheric stressing of a magnetic arcade is incapable of producing phenomena such as prominence eruption or coronal heating. Some critical ingredient is missing from this model. There are several possibilities. One is that emerging flux plays the dominant role in activating the coronal magnetic field. Simulation which allow for flux emergence and submergence need to be considered. Another possibility is that a complex magnetic topology is required. We have argued (Antiochos 1989,1990) that a pure dipolar field (i.e., one due to a single positive and a single negative polarity region on the photosphere) is somewhat pathological, since it is the only field with a well-behaved connectivity everywhere. In a more realistic field which is due to a number of different polarity regions at the photosphere, the connectivity must be discontinuous

and null points must occur in the corona. In this case current sheets and reconnection will readily occur as a result of footpoint motions. We are currently pursuing these possibilities.

In summary, we believe that the work reported here constitutes only a first step in examining the 3D dynamics of coronal magnetic fields. Much more interesting simulations await to be done.

APPENDIX

COMPUTATIONAL PROCEDURE

We modify the algorithm of Zang and Hussaini (1986) to include magnetic field terms. The governing equations 1 - 5 are solved within the computational range Ω by means of the following time-step splitting:

$$\mathbf{v}_t^* = \mathbf{v}^* \times \boldsymbol{\omega}^* + \mathbf{j}^* \times \mathbf{B}^* + \frac{1}{M}\nabla^2 \mathbf{v} \qquad (in\ \ \Omega)$$

$$\mathbf{A}_t^* = \mathbf{v}^* \times \mathbf{B}^* - \frac{1}{S}\nabla \times \nabla \times \mathbf{A} \qquad (in\ \ \Omega)$$

$$\mathbf{v}^* = \mathbf{g}^* \qquad (on\ \ \partial\Omega)$$

$$\mathbf{A}^* = \mathbf{h}^* \qquad (on\ \ \partial\Omega)$$

$$\mathbf{v}^*(\mathbf{x}, t_n) = \mathbf{v}(\mathbf{x}, t_n) \qquad (in\ \ \Omega)$$

$$\mathbf{A}^*(\mathbf{x}, t_n) = \mathbf{A}(\mathbf{x}, t_n) \qquad (in\ \ \Omega)$$

$$\mathbf{v}_t^{**} = -\nabla P^{**} \qquad (in\ \ \Omega)$$

$$\nabla \cdot \mathbf{v}^{**} = 0 \qquad (in\ \ \Omega)$$

$$\mathbf{v}^{**} \cdot \hat{\mathbf{n}} = \mathbf{g} \cdot \hat{\mathbf{n}} \qquad (on\ \ \partial\Omega)$$

$$\mathbf{v}^{**} \cdot \hat{\tau} = -\nabla P^{**} \cdot \hat{\tau} \qquad (on\ \ \partial\Omega)$$

$$\mathbf{v}^{**}(\mathbf{x}, t^*) = \mathbf{v}^*(\mathbf{x}, t^*) \qquad (in\ \ \Omega)$$

The first time-level, represented by single-starred variables, is a convective, dissipative step. The second level, represented by double-starred variables, is a pressure step which enforces the solenoidality of the flow field.

A staggered grid is employed using the following collocation points: $x_i = 2\pi i/N_x$ for $i = 0, 1, N_x - 1$, $y_j = 2\pi j/N_y$ for $j = 0, 1, N_y - 1$, $z_k = \cos(\pi k/N_z)$ for $k = 0, 1, N_z$, and, $z_{k+1/2} = \cos[\pi(k + 1/2)/N_z]$ for $k = 0, 1, N_z - 1$. Velocities and vector potentials are defined at the nodes (x_i, y_j, z_k). Pressures are defined at the shifted points $(x_i, y_j, z_{k+1/2})$.

ACKNOWLEDGEMENTS

The numerical simulations reported here were performed on the NASA Ames Research Center Cray supercomputers under a grant from the Numerical Aerodynamic Simulation Program and on the NRL Cray X-MP under a grant of time from the NRL 6.1 Production Run program. This work was supported by the NASA Space Physics Theory Program and the Office of Naval Research. We thank Drs. R. Ramamurti, J. H. Gardner, and J. P. Dahlburg for helpful conversations.

REFERENCES

Aly, J. J. 1984, *Ap. J.*, **283**, 349.

Antiochos, S. K. 1987, *Ap. J.*, **312**, 886.

Antiochos, S. K. 1989, *Solar and Stellar Flares, I.A.U. Coll. 104, Poster Papers* (eds. B. Haisch and M. Rodono), 277.

Antiochos, S. K. 1990, *Memorie della Societa Astronomica Italiana*, (ed. G. Poletto), in press.

Dahlburg, R. B., Zang, T. A., Montgomery, D., and Hussaini, M. Y. 1983, *Proc. Natl. Acad. Sci.*, **80**, 5798.

Dahlburg, R. B., Zang, T. A., and Montgomery, D. 1986, *J. Fluid Mech.*, **169**, 71.

Dahlburg, R. B., Dahlburg, J. P., and Mariska, J. T. 1988, *Astr. Ap.*, **198**, 300.

Dahlburg, R. B., and Picone, J. M. 1989, *Phys. Fluids B*, **1**, 2153.

Démoulin, P., and Priest, E. R. 1989, *Astr. Ap.*, **214**, 360.

Greene J. 1988, *J. Geophys. Res.*, **93**, 8583.

Kippenhahn, R., and Schlüter, A. 1957, *Zs. Ap.*, **43**, 36.

Kuperus, M., and Raadu, M. A. 1974, *Astr. Ap.*, **31**, 189.

Mikič, Z. 1990, *Phys. Fluids B*, **2**, 1450.

Mikič, Z., Barnes, D. C., and Schnack, D. D. 1988, *Ap. J.*, **328**, 830.

Mikič, Z., Schnack, D. D., and Van Hoven, G. 1989, *Ap. J.*, **338**, 1148.

Moore, R. 1988, *Ap. J.*, **324**, 1132.

Orszag, S. A., and Tang, C.-M. 1979, *J. Fluid Mech.*, **90**, 129.

Parker, E. N. 1972, *Ap. J.*, **174**, 499.

Parker, E. N. 1979, *Cosmical Magnetic Fields*, (Oxford: Clarendon Press).

Parker, E. N. 1987, *Ap. J.*, **318**, 876.

Pneuman, G. W. 1983, *Solar Phys.*, **88**, 219.

Priest, E. R. 1982, *Solar Magnetohydrodynamics*, (Dordrecht: Reidel).

Sakurai, T. 1979, *Pub. Astr. Soc. Japan*, **31**, 209.

Sturrock, P. A. 1989, *Sol. Phys.*, **121**, 387.

Strauss, H. and Otani, N. 1988, *Ap. J.*, **326**, 418.

Tandberg-Hanssen, E. 1974, *Solar Prominences*, (Dordrecht: Reidel).

van Ballegooijen, A. A. 1988 *Geophys. Astrophys. Fluid Dyn.*, **41**, 181.

van Ballegooijen, A. A. and Martens P.C.H. 1989, *Ap. J.*, **343**, 971.

Velli, M., and Hood, A. W. 1986, *Solar Phys.*, **106**, 353.

Yang, W. H., Sturrock, P. A., and Antiochos, S. K. 1988, *Ap. J.*, **309**, 383.

Zang, T. A., and Hussaini, M. Y. 1986, *Appl. Math. Comp.*, **19**, 359.

PHOTOSPHERIC FLOW FIELD

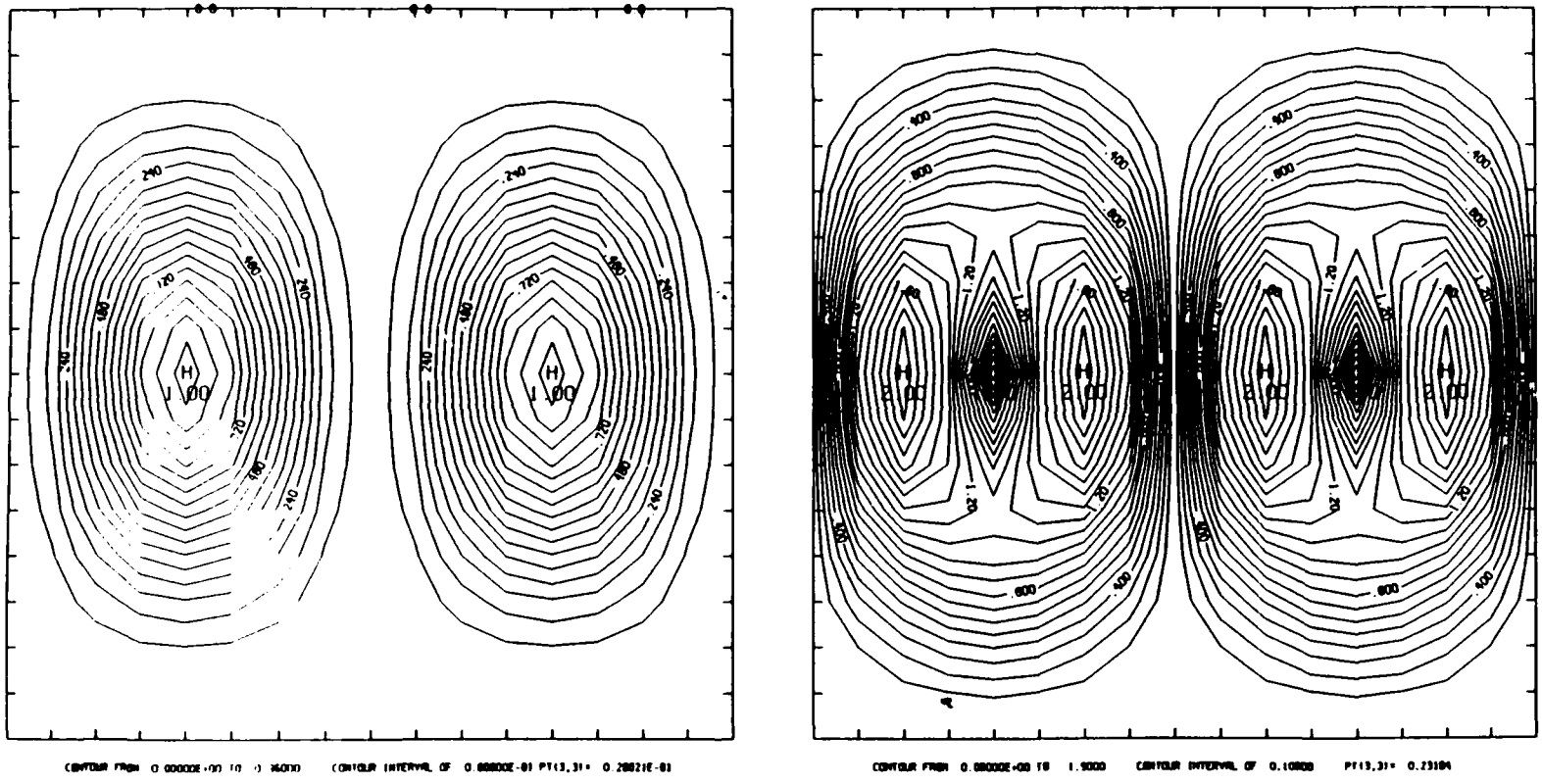

(a) (b)

Fig. 1 — One quadrant of the photospheric flow field given in equation 4, with $C = 1$. (a) Stream function $\psi = -\sin^2 2x \sin^3 y$. Note the presence of an X type neutral line in the center of the flow pattern, running along the magnetic neutral line. (b) Velocity magnitude $|\mathbf{v}| = [(\partial\psi/\partial x)^2 + (\partial\psi/\partial y)^2]^{\frac{1}{2}}$.

NORMAL MAGNETIC FIELD AT PHOTOSPHERE

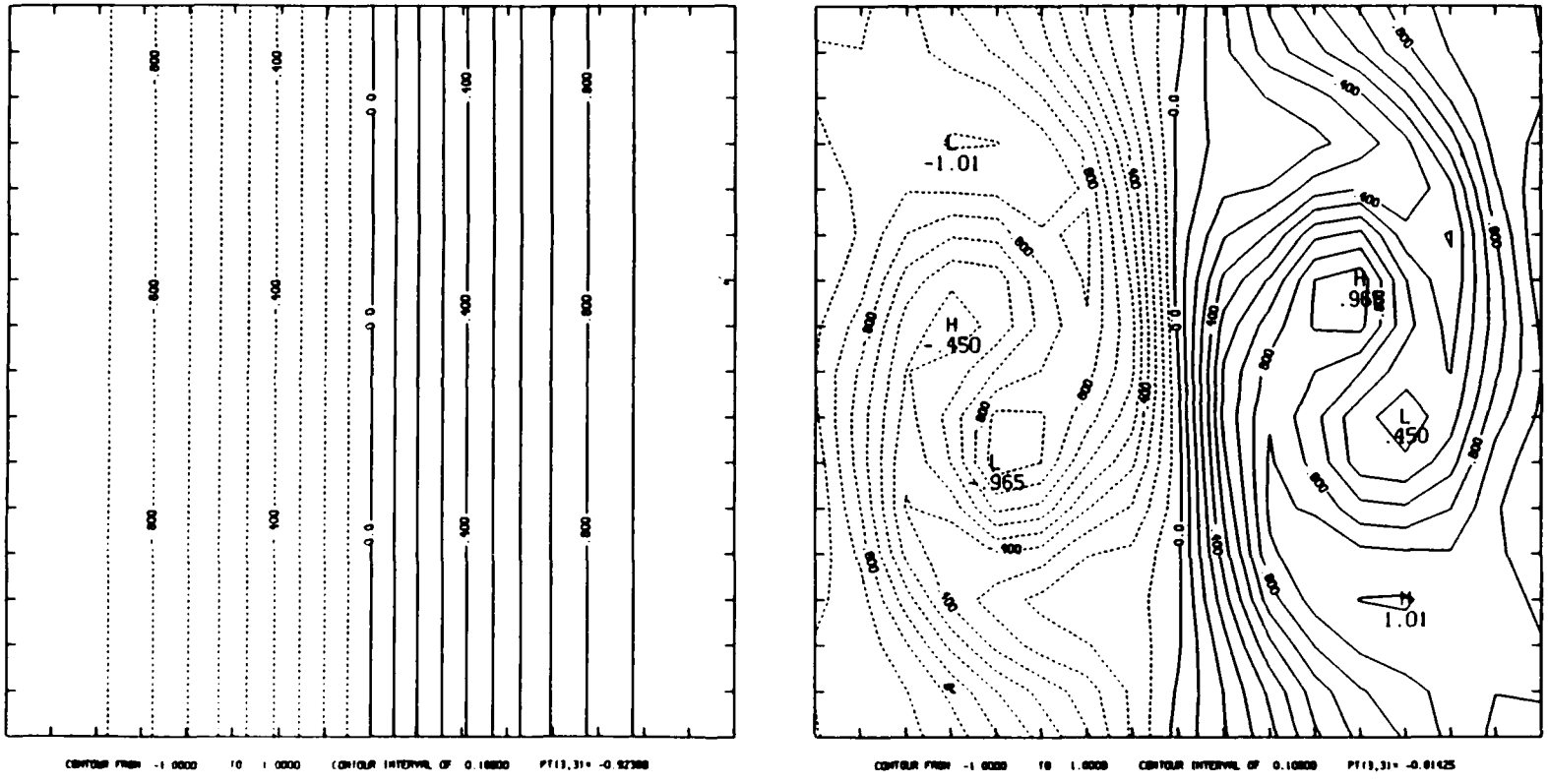

(a) (b)

Fig. 2 — One quadrant of the normal magnetic field in the photosphere. The same quadrant is shown in Fig. 1. (a) $t = 0\tau$, initial conditions. (b) $t = 10\tau$, conclusion of the twisting phase. The figure shows how much the magnetic field is twisted from its initial configuration, approximately one full rotation. After $t = 10\tau$, the photospheric B_z retains this form.

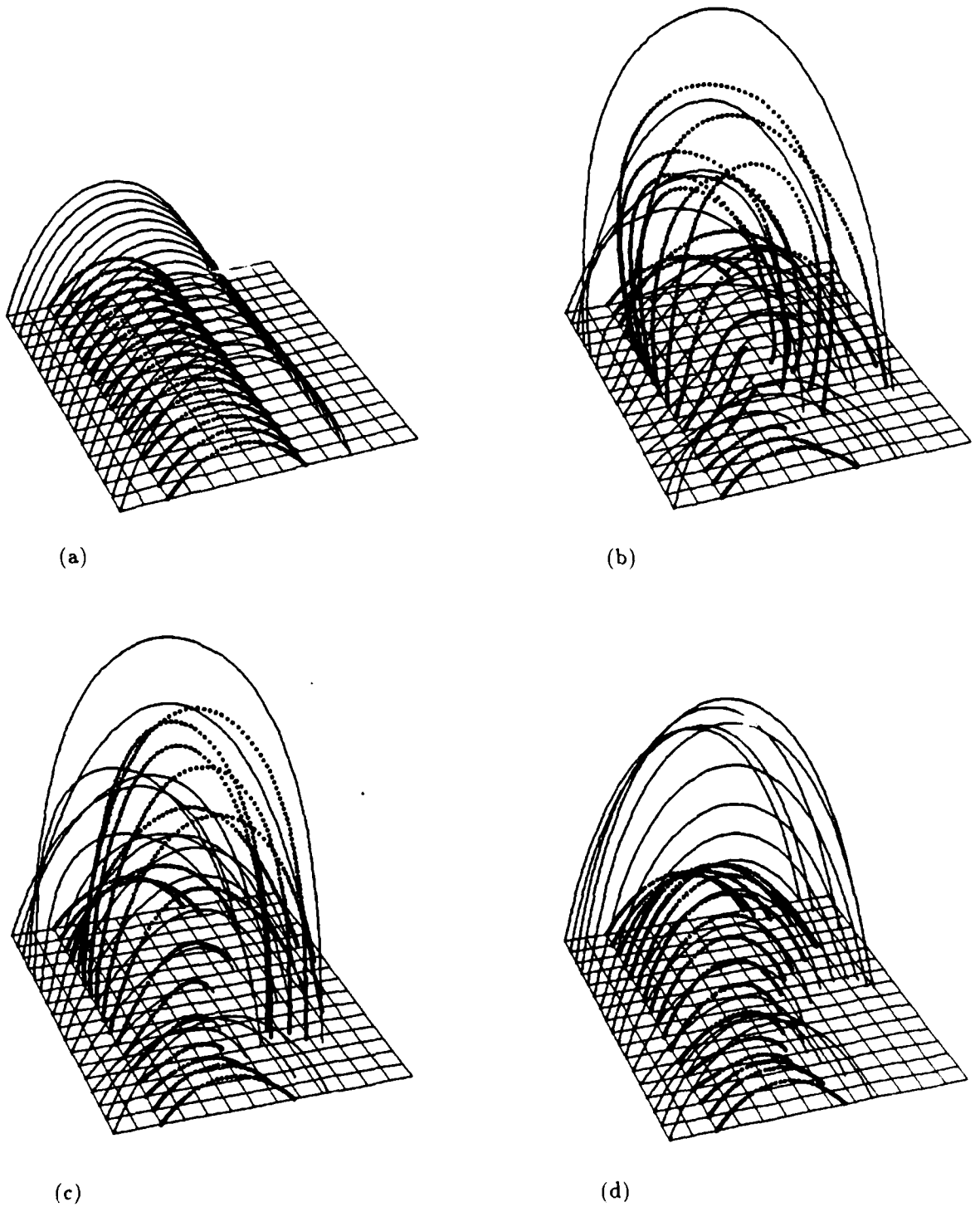

Fig. 3 — One quadrant of magnetic field lines, side view. The same quadrant is shown as in Fig. 1. (a) $t = 0\tau$, initial conditions. (b) $t = 10\tau$, conclusion of the twisting phase. (c) $t = 20\tau$, partial damping. (d) $t = 70\tau$, conclusion of the simulations.

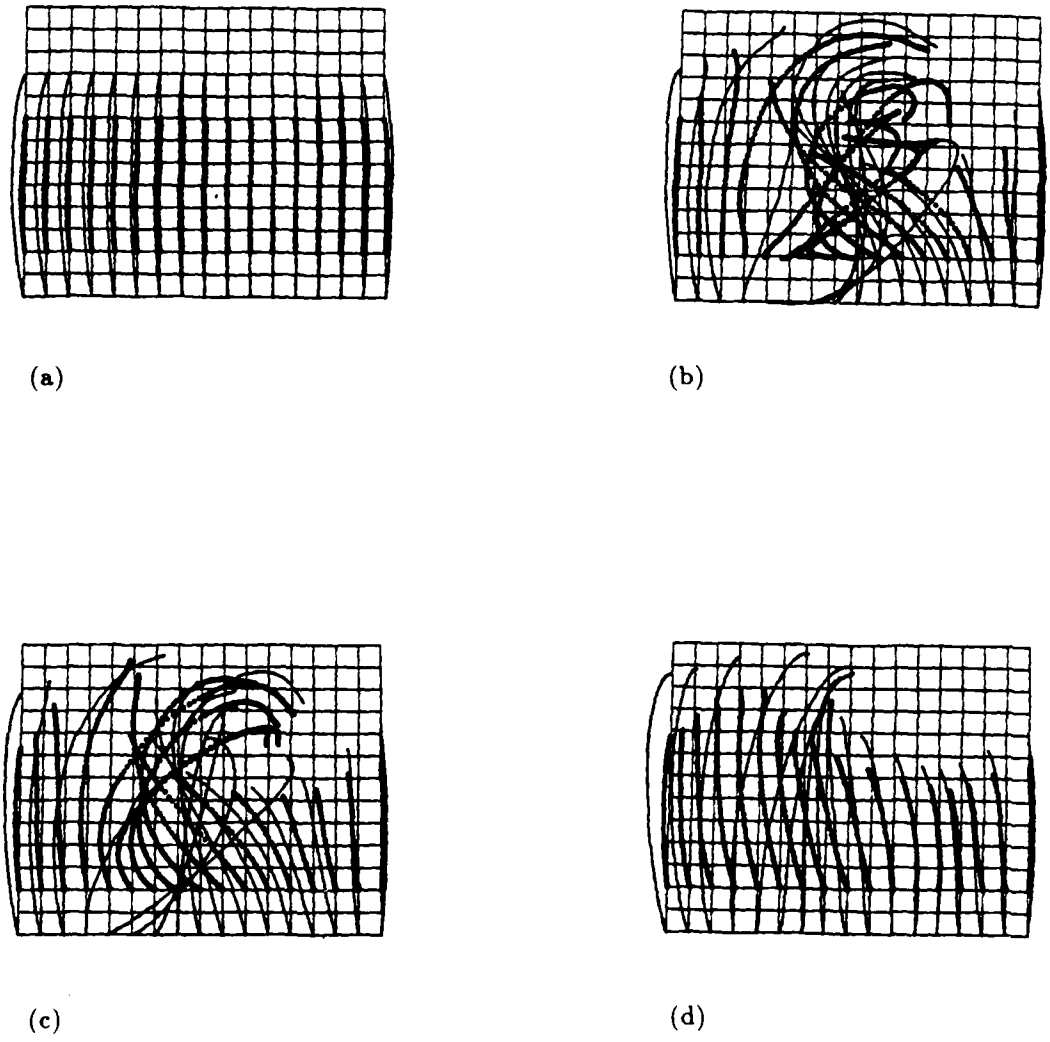

Fig. 4 — One quadrant of magnetic field lines, top view. The same quadrant is shown as in Fig. 1. (a) $t = 0\tau$, initial conditions. (b) $t = 10\tau$, conclusion of the twisting phase. (c) $t = 20\tau$, partial damping. (d) $t = 70\tau$, conclusion of the simulations.

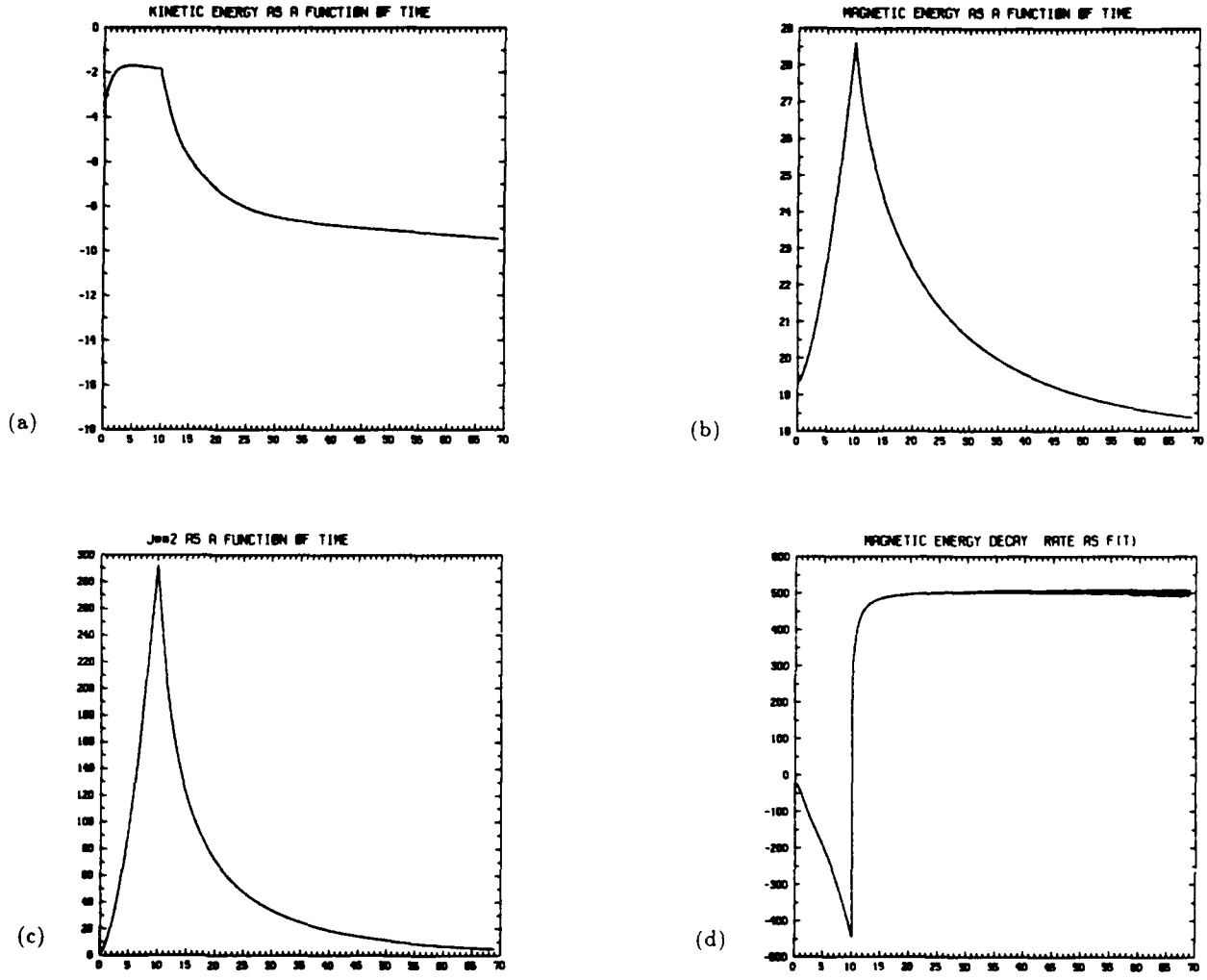

Fig. 5 — Global quantities versus time. (a) logarithm of kinetic energy ($1/2 < |\mathbf{v}|^2 >$). (b) magnetic energy ($1/2 < |\mathbf{B}|^2 >$). (c) mean square electric current ($1/2 < |\mathbf{j}|^2 >$). (d) mean magnetic Lundquist number

$$S(t) = -\frac{2 < |\mathbf{j}|^2 >}{\frac{d}{dt} < |\mathbf{B}|^2 >}.$$